Experiments on single oblique laminar-instability waves in a boundary layer: Introduction, growth, and transition

Steven P. Schneider[a] and Donald Coles
Graduate Aeronautical Laboratories, California Institute of Technology, Pasadena, California 91125

(Received 11 November; accepted 10 September 1993)

The laminar–turbulent transition in an incompressible flat-plate boundary layer was studied experimentally by using a spanwise array of computer-controlled surface heating elements to generate small disturbances. Oblique Tollmien–Schlichting waves were successfully introduced, and their downstream development into the intermittent region was studied using flush-mounted hot-film wall-shear sensors and dye flow visualization. Comparative studies of the development of single oblique waves were made for various wave angles, frequencies, and amplitudes. As these single oblique waves grew and began to break down, higher harmonics and subharmonics appeared in the wall shear. The amplitude of the subharmonic component decreased rapidly with increasing oblique-wave angle, so that a 10° oblique wave had a subharmonic amplitude an order of magnitude below that for a two-dimensional (2-D) wave. Thus, the nonlinear mechanism that produces the subharmonic is affected by the symmetry of the primary wave. Intermittency measurements, carried out farther downstream, show that a 2-D wave is most effective in moving the transition point upstream, for a given power input.

I. INTRODUCTION

Recent reviews of the extensive literature of transition in wall-bounded shear flow can be found in Herbert[1] and Kleiser and Zang.[2] The transition process in the boundary layer occurs over an extended streamwise distance, which can be divided into linear, nonlinear, and intermittent regions. Even if the process is initially two dimensional, as is often assumed, the development of three-dimensionality in the nonlinear region is crucial to the onset of intermittency and turbulence.

Development of three-dimensionality has recently been the subject of a great deal of research. Much of this work involves the study of the nonlinear breakdown of large-amplitude 2-D primary waves. The main result is an accepted interpretation of the nonlinear breakdown of such waves in terms of two principal mechanisms. These are shown in Fig. 1, taken from Bertolotti (Ref. 3, Figs. 6.1 and 6.2). Both parts of the figure show streaklines simulated using a flow field computed from Floquet-based secondary instability theory. The simulated smoke wire is located at the critical layer, and the Reynolds number is 620. In both cases, the flow field contains two disturbances: one a 2-D instability wave of specified frequency and amplitude, and the other a 3-D mode with specified spanwise wave number, frequency, and amplitude. In both cases, the spanwise-varying disturbances eventually become Λ-shaped structures that lead to local turbulence.

In the upper part of Fig. 1, the 3-D mode is chosen to reflect the K-type secondary instability, in which the spanwise disturbances are aligned in rows. This instability was first studied by Klebanoff *et al.*,[4] and is characterized by the evolution of strong local three-dimensionality in a system of spanwise alternating peaks and valleys (maxima and minima in the amplitude of the streamwise fluctuation). In the lower part of Fig. 1, the 3-D mode is chosen to reflect the H-type secondary instability, in which the spanwise disturbances are arranged in a staggered pattern. The K-type and H-type instabilities are named after Klebanoff and Herbert. A similar staggered pattern has been observed in the secondary instability of laminar circular cylinder wakes (Ref. 5, Fig. 20). This instability yields a characteristic subharmonic frequency in measurements made at a fixed location. The staggered pattern can be explained using either the secondary instability theory mentioned, or, using the idea of resonance between a primary 2-D instability wave and a pair of oblique instability waves of equal and opposite angle.[6] In the latter case, the subharmonic instability is called the C type (for Craik). Experiments confirming the presence of subharmonics under certain conditions were first performed by Kachanov and Levchenko (see, e.g., Ref. 7).

When 2-D waves are introduced in a controlled way, the particular nonlinear breakdown pattern that occurs in a given flow depends on the amplitude and pattern of 3-D disturbances present in the background noise. Herbert has reviewed the extensive research into the characteristics of these two patterns up to 1988,[1] and work in this area is continuing.[8] In all cases where study of the staggered pattern involves oblique waves, a pair of oblique waves of equal and opposite angle is specified. Such pairs of oblique waves are equivalent to disturbances that vary sinusoidally with the spanwise direction in a symmetric and periodic way.

In the present paper we address a different topic; namely, the breakdown of large-amplitude single *oblique* primary waves. This flow is no longer spanwise symmetric, although it is still spanwise periodic. Slightly oblique waves have nearly the same amplification as 2-D waves, and thus are likely to occur in practice.[9] In fact, a slight asymmetry in the flow might make single oblique waves of small angle

[a]Present address: School of Aeronautics and Astronautics, Purdue University, West Lafayette, Indiana 47907-1282.

 1070-6631/94/6(3)/1191/13/$6.00

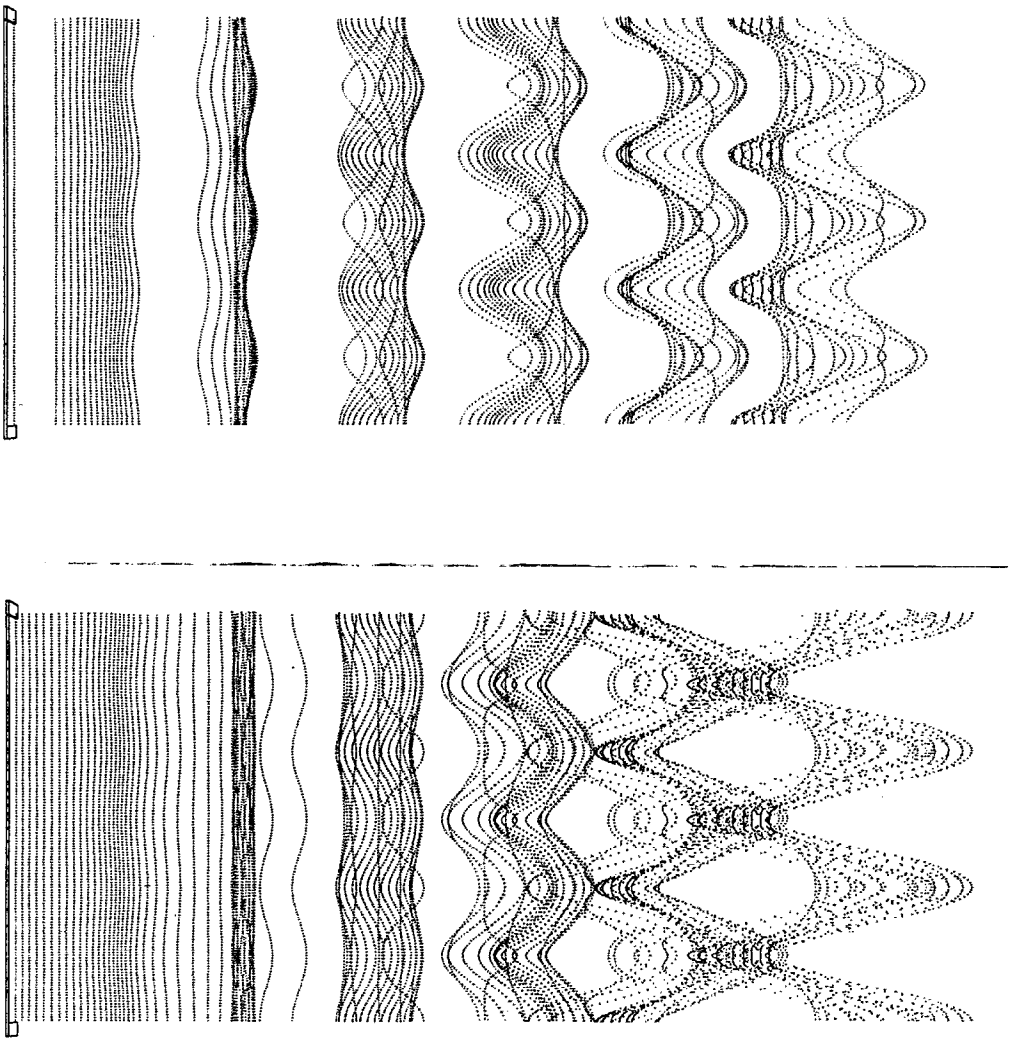

FIG. 1. Streaklines depicting accepted models of nonlinear breakdown. Upper image: K type. Lower image: H type. Flow is from left to right.

a dominant feature. Small changes in the end conditions have been observed to induce oblique vortex shedding in the wake of a circular cylinder, even when the length-to-diameter ratio is 100 or more.[10]

Both of the secondary breakdown patterns sketched in Fig. 1 rely on the two-dimensionality of the primary instability wave. The effect of primary-wave obliquity on nonlinear development and breakdown has not been a subject of study, to our knowledge, except for the work of Robey.[11] The experiments reported here were undertaken to explore this effect. These single oblique waves are also of interest because they are a standard simple three-dimensional wave form. For example, the spatially localized small disturbances studied by Gaster[12] can be described in terms of packets of single oblique instability waves using Fourier decomposition techniques. Oblique waves have also been observed near the wing tips of the turbulent spot.[13] These single oblique waves are solutions of linearized disturbance equations with straight but oblique constant-phase lines (see Fig. 2). Soon after the development of the linear theory, Squire[14] derived a transformation that showed that the eigenvalues of an oblique wave are equal to the eigenvalues

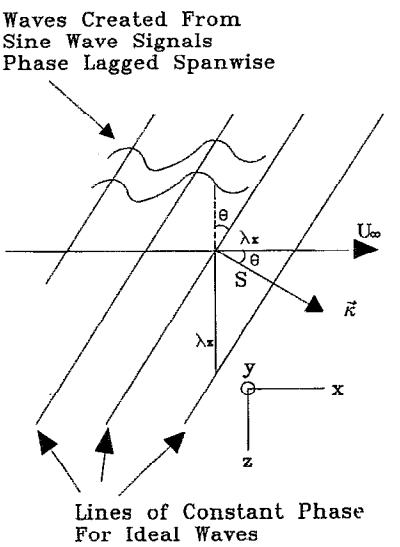

FIG. 2. Oblique wave geometry.

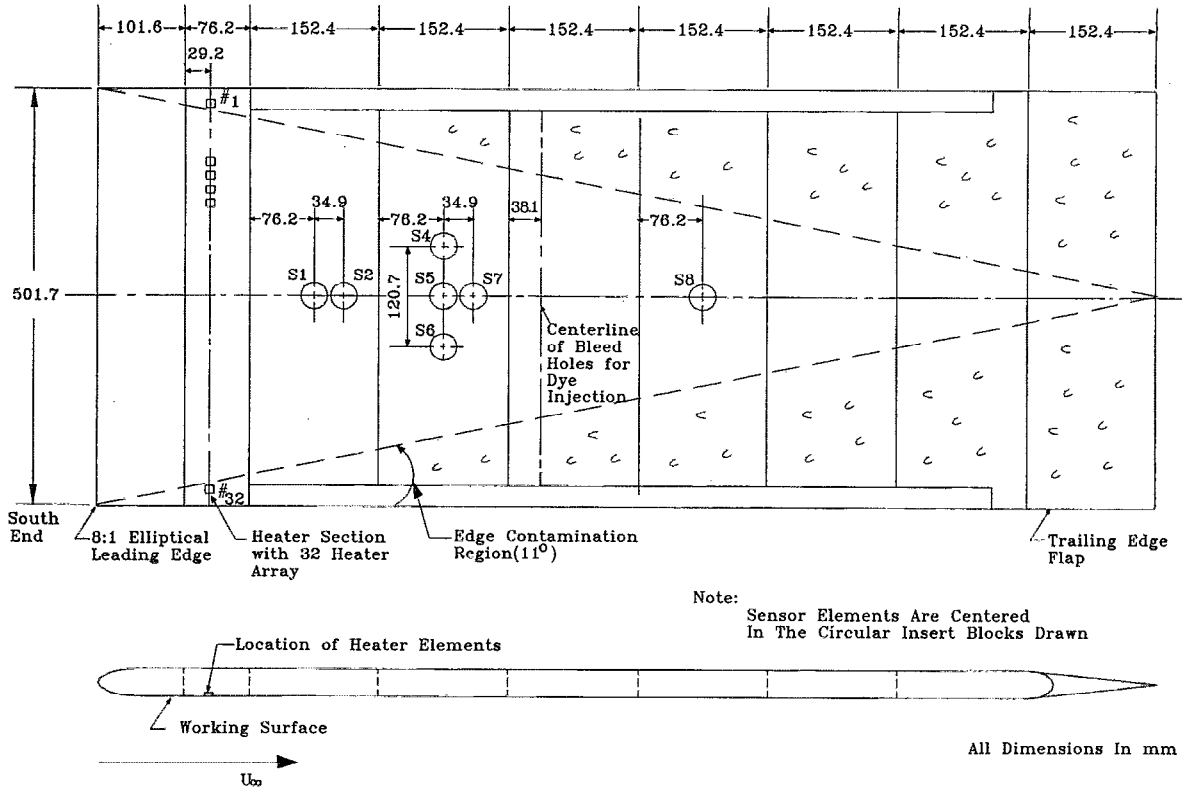

FIG. 3. Schematic drawing of flat-plate model.

of an equivalent 2-D wave at a lower Reynolds number. Thus, the mode that is first unstable is a 2-D mode.

However, oblique waves are not just a trivial rotation of 2-D waves. These waves contain all three components of both velocity and vorticity (Craik[15]). The vortex lines for the oblique waves are distorted helices, with the helical axes parallel to the constant phase lines and the pitch of the helix windings decreasing from infinity as the oblique wave angle is increased from zero (Robey,[11] Fig. 5). These fully 3-D vortex lines are now directly subject to stretching and tilting, unlike 2-D vortex lines. Moreover, the maximum of the vorticity moves away from the wall as the oblique wave angle is increased.[16,17]

In the work reported here, single oblique waves were generated and their development was studied all the way into the intermittent region. This work is the first systematic study of the generation and growth of such waves, because of the difficulty of generating them experimentally. Some experiments have been reported in which such waves were introduced by a wavemaker that was not normal to the free-stream velocity (see Kachanov[17] and Kendall,[18] who give linear growth results for a few wave angles). This method has two drawbacks. First, the wave is introduced at a streamwise position that varies with spanwise position, so that the amplification history of the wave will vary across the span. Second, the oblique angle can be varied only with difficulty. Explicit computations of linear instability of waves of finite length, introduced by an oblique line source, have been reported by Mack (Ref. 19, Fig. 6). These computations show a severe distortion of the wave fronts at all spanwise locations, except for a small region immediately downstream of the center of the wavemaker. This result suggests that the spanwise differences in Reynolds-number history encountered by such a wave might be important. Robey's method[20] of generating the oblique waves produces them entirely at one streamwise position, and so avoids these difficulties.

The apparatus described in Sec. II was used to introduce single oblique waves of various angles, frequencies, and amplitudes. A comparative study of the effect of these parameters on oblique wave development was made. It should be emphasized that the main purpose of the experiments was to determine the trends and effects observed when the angle of the oblique instability waves was varied. The focus of the experiments is therefore on comparisons among the different cases.

II. EXPERIMENTAL APPARATUS

The main element of the work described here is an improved version of Robey's discrete heater apparatus for introducing controlled three-dimensional disturbances into a laminar boundary layer. A flat-plate model mounted in a water tunnel is used to form the boundary layer used as a basis for study. A flush-mounted array of 32 small individual heating elements spanning the width of the boundary layer allows the introduction of three-dimensional perturbation patterns, as shown in Fig. 3. If sine waves of uniform frequency, amplitude, and phase are introduced into the heaters, the heaters will all act in unison to produce a

nominally two-dimensional instability wave. However, if a uniform phase lag is introduced in the signals between adjacent heaters, the instability wave pattern produced will have constant phase lines that are delayed between one side of the plate and the other; i.e., the pattern will be a single oblique wave train (see Fig. 2). Robey's technique has also been adapted for use in shear layers (see Nygaard and Glezer[21]).

Corke and Mangano[8] have also developed a discrete array disturbance generator, as have Meier *et al.*[22] The perturbation apparatus used here is, however, different from that used by Corke. The present apparatus works in water as opposed to air; it is completely nonintrusive; and it is fabricated using photolithography. In practice, it is used to introduce sine-wave perturbations, as opposed to the simpler square-wave perturbations used by Corke.

The phase increment between adjacent heaters could be varied from zero to about one-fourth of the wave period, but was kept small to improve the quality of wave generation. The difference between the ideal wave and the discretely generated wave can be represented as a Fourier series in time and in space. It was expected that any higher harmonics that might be generated would decay rapidly as the wave travels downstream. This expectation was fulfilled, since no harmonics were ever apparent in the wall shear traces at the first measuring station downstream, or in the spanwise cross-correlations that will be discussed below. Recent computational results obtained by Kral (Ref. 23, p. 165) also indicate that these higher harmonics decay rapidly. Finally, experiments with more complicated wave patterns[24] showed that short-wavelength perturbations to oblique waves produced no apparent effects in the wall shear traces at the first sensor location downstream.

All the experiments were performed in the Free Surface Water Tunnel of the Hydrodynamics Laboratory at GALCIT (Graduate Aeronautical Laboratories, California Institute of Technology; see Ward[25]). The tunnel was operated as an open channel flow for these experiments. It has a 508 mm wide test section with Plexiglas walls on three sides. The turbulence level in the test section was less than 0.15%. The unforced boundary layer was laminar to above $\mathrm{Re}_x = 1.4 \times 10^6$, according to flow visualization with dye seeped in at the wall. Figure 4 shows the power spectrum of the free-stream turbulence, which was approximately $1/f$ for low frequencies. Further details regarding the experimental apparatus and conditions can be found in Ref. 26.

A modular flat-plate model was fabricated for the experiments (see Fig. 3). The plate spanned the width of the test section, and was always located horizontally in the same position in the center of the test section. The flat plate was carefully aligned parallel to the flow, and the variation of the pressure coefficient over the rear two-thirds of the plate was less than 0.04. Local pressure-gradient effects near the 8:1 elliptical leading edge of the plate were computed using an inviscid surface-panel method. Hess and Smith[27] confirm that the pressure coefficient in attached flows with thin boundary layers can readily be calculated using this technique. They provide comparisons with ana-

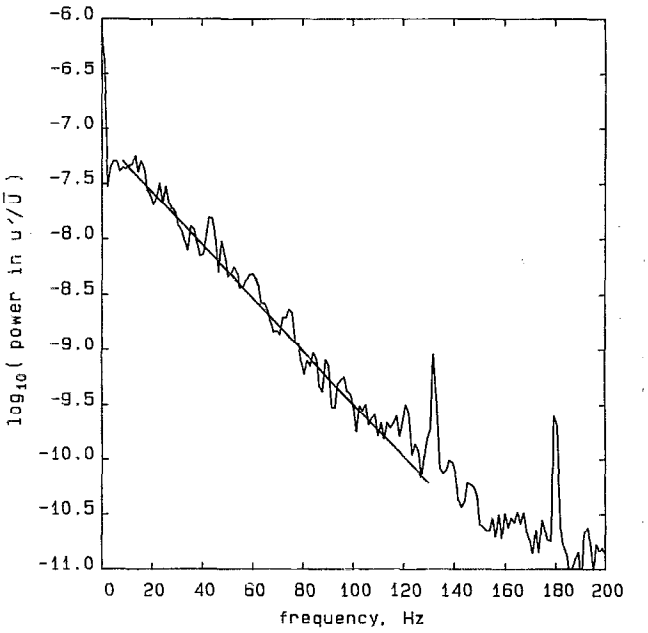

FIG. 4. Spectrum of free-stream turbulence in FSWT; $u'_{\mathrm{RMS}}/\bar{U} = 0.15\%$ in the frequency range 0.2–2500 Hz.

lytic solutions and experimental data. The computations agree with theory to within less than 1% in the pressure coefficient. Experimental data is limited, but agreement to within apparent experimental scatter is shown for various bodies in their paper. The results obtained here agree with Fig. 58 in the paper of Hess and Smith. The boundary-layer thickness was then computed from laminar boundary-layer theory (Ref. 28, p. 269).

The wave-generating circuitry supplied zero offset sine waves to the heater array. A custom-built heater-signal controller generated 32 individual sine waves for the voltage on the 32 heaters. The amplitude of the sine wave on each heater could be selected from a set of 16 values, and the phase lag of the signal between one heater and the next could also be selected from a set of 16 values. The controller was able to generate wave angles from zero to about 32°. A 32-channel power amplifier supplied power gain to the signals from the controller and drove the heater array. The power applied to the various heaters was uniform to within about one percent, for a given setting of wave angle, independent of frequency. This applied power was also independent of wave angle, except for the in-phase 2-D waves, when it was reduced about 13% due to increased I^2R dissipation in the ground bus. Although the power delivered to the heaters could be held constant, the power delivered to the flow could vary with the forcing parameters due to receptivity effects. The consistency of the phase shifts between signals to adjacent heaters was within about one percent of the specified individual phase shift, except for the smallest oblique wave angles, for which the mean phase shift was itself very small.[26] Since the signal placed on the heaters is a sine wave in voltage, and the heating power is proportional to the square of the voltage, the heating fluctuations occur at twice the frequency of the voltage fluc-

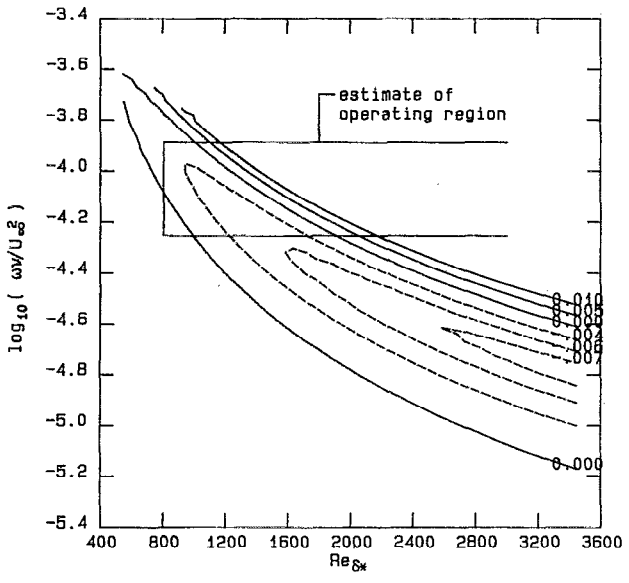

FIG. 5. Contours of linear amplification rate for parallel flow, from data provided by Mack.

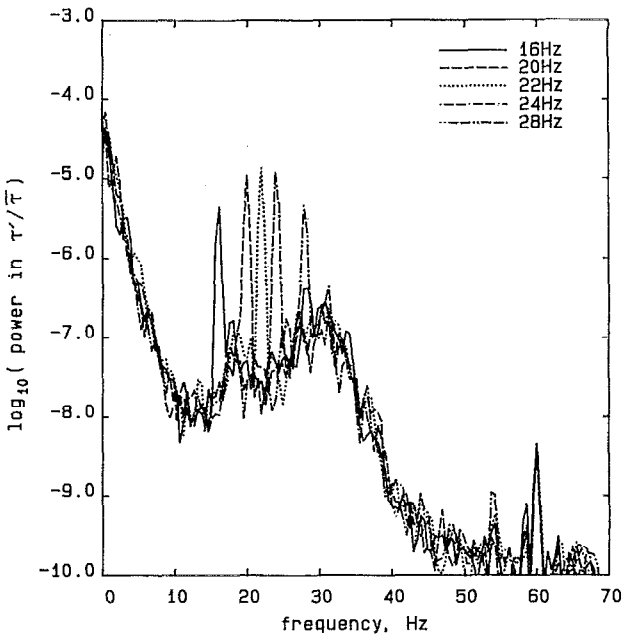

FIG. 6. Wall-shear spectra in linear region at $Re_{\delta*}=1100$. Five spectra for different heating frequencies (83 W total power, sensor S1, 2-D forcing, $U_\infty=1.12$ m/s).

tuations. The forcing frequencies reported here are the frequencies of the heating power.

Hot-film wall-shear sensors were used as the principal flow diagnostic. The locations of the sensors are shown in Fig. 3. The notation "*Sn*," where "*n*" is an integer, is used to refer to data obtained from a sensor positioned as shown in Fig. 3. The hot-film sensors were calibrated before and after each set of experiments, using the standard procedures outlined by Brown.[29] For each calibration, the fit between the sensor data and the theoretical calibration law was good. However, a slow drift was often observed to occur during the six to twelve hours required for a set of experiments. This drift (typically 3%–10%) prevented the accurate measurement of local growth rates using the different fixed sensors.

The amplification rates given by linear instability theory for 2-D waves in a zero-pressure-gradient boundary layer at various frequencies and Reynolds numbers are plotted in Fig. 5. The computations assume parallel flow and spatial growth, and were supplied by Mack,[30] whose computational method is described in Ref. 19. The operating region for the work reported here is sketched in the figure, with the beginning of the operating region corresponding to the heater-array location. The free-stream velocity used for normalization is the most common one; namely, $U_\infty=1.12$ m/s.

III. LINEAR OBLIQUE WAVES

Since the waves are introduced with small amplitude, the region immediately downstream of the source is the site of linear growth and interaction phenomena. A shear trace was said to belong to this linear region if its spectrum contained a peak only at the primary forcing frequency. Typical linear spectra can be seen in Fig. 6, which shows five spectra for waves forced at five different frequencies in separate experiments. The response to the forcing shows up as sharp peaks, whose amplitude varies with the forcing frequency. Although the word "amplitude" is used in referring to the strength of the instability waves, the spectra themselves are always plotted in terms of the *power* in the instability-wave shear trace. Thus, the amplitude of the 22 Hz peak in Fig. 6 is about $\tau'/\bar{\tau}=0.3\%$, since the power spectrum shows that $\tau'^2/\bar{\tau}^2=10^{-5}$.

A. Wave amplitudes

Wave amplitudes are given here in terms of the amplitude of the wall shear fluctuations. Robey (Ref. 31, p. 12) gives theoretical arguments and experimental data to show that

$$\tau'/\bar{\tau}\approx\tfrac{5}{2}(u'_{\max}/U_\infty),$$

where $u'_{\max}$ is the local maximum of the streamwise fluctuation velocity and U_∞ is the free-stream velocity. Of course, this result will vary with the shape of the wave eigenfunction in a sometimes dramatic way that can be examined theoretically (see Ref. 32).

Although the emphasis of this work is on qualitative effects of the primary-wave obliqueness, comparisons of the observed wave growth with theory may still be of interest. Theoretical growth rates for 2-D waves in parallel flow have therefore been computed using Gaster's zero-pressure-gradient program,[33] and also using an Orr–Sommerfeld solver.[34] Integrated growth rates have been computed following Mack (Ref. 35; also see Ref. 24). The results of the two methods agree very well with each other and also with the data published by Mack (Fig. 6.4 in Ref. 35). Figure 7 shows the experimental results for the growth between sensors S1 and S2F for three levels of

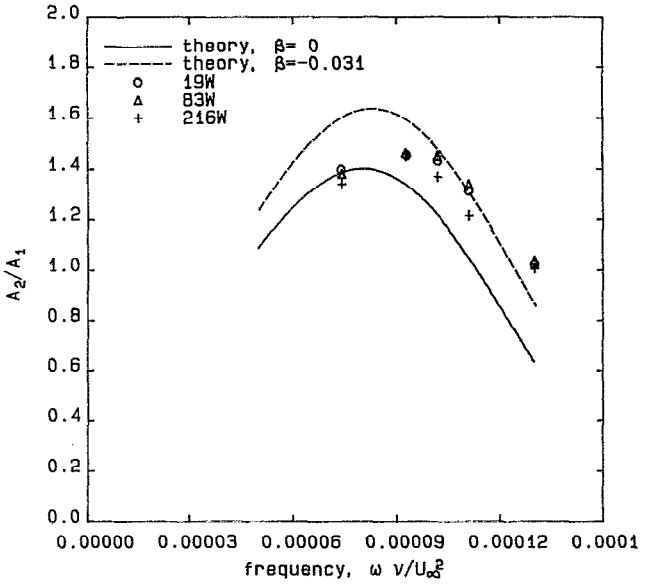

FIG. 7. Linear wave amplification compared to theory. 2-D wave growth between $Re_{\delta^*}=1090$ and $Re_{\delta^*}=1150$.

wave-generation power. The suffix "F" indicates that sensor S2F is located 2.5 mm forward of the center of the location marked for sensor S2 in Fig. 3. The vertical axis gives A_2/A_1, where A_2 is the RMS wave amplitude at the forcing frequency at sensor S2F, and A_1 is the wave amplitude at sensor S1. Here, Re_{δ^*} is the Reynolds number based on free-stream conditions and the local displacement thickness. The theory is computed both for zero pressure gradient and for an adverse pressure gradient with a Falkner–Skan β of -0.031, as calculated for the region between the two sensors by the panel-method and boundary-layer computation already mentioned. The experimental growth rates fall between the two theoretical curves. The most amplified frequency in the data is slightly higher than that in either theoretical curve. The early experiments by Schubauer and Skramstad[36] also suggest that higher frequencies are more amplified than would be expected according to parallel-flow linear theory. The qualitative agreement is typical of experimental studies at low Reynolds numbers.[37] Experimental work seeking precise agreement with the linear flat-plate instability theory remains a topic for future research, even for the 2-D case.

B. Phase speeds

Phase speeds for oblique waves can be defined using the relation

$$\mathbf{c}_{\text{phase}}=\frac{\omega}{(|\boldsymbol{\kappa}|)^2}\boldsymbol{\kappa},$$

where $\boldsymbol{\kappa}$ is the wave vector for the wave (see Whitham,[38] p. 365). For spatially growing oblique waves with fluctuation velocity,

$$\mathbf{u}=\Re[\mathbf{u}(y)e^{i(\alpha x+\beta z+\omega t)}],$$

where β and ω are real, we have that

$$\boldsymbol{\kappa}=\alpha_r\mathbf{i}+\beta\mathbf{k},$$

where x is the streamwise coordinate, z is the spanwise coordinate, y is the coordinate perpendicular to the wall, α_r is the real part of the complex number α, $\mathbf{i}$ and $\mathbf{k}$ are unit vectors in the x and z directions, and $\Re$ is the real part of the argument. This case is called the spatial case, since the waves are uniform in time and grow or decay in the downstream direction. The phase speed in the spatial case is therefore

$$\mathbf{c}_{\text{phase}}=\frac{\omega\alpha_r\mathbf{i}+\omega\beta\mathbf{k}}{\alpha_r^2+\beta^2}.$$

However, the component of the phase speed vector in the x direction does not give the speed of the constant phase lines along the x direction. The formula for the speed of constant phase lines in the x direction (called the "phase speed in the x direction" or $c_{\text{phase},x}$ here), can be easily derived from first principles, and is

$$c_{\text{phase},x}=\frac{\omega}{\boldsymbol{\kappa}\cdot\mathbf{i}}$$

or

$$c_{\text{phase},x}=\frac{\omega}{\alpha_r}.$$

This phase speed in the x direction was measured in the experiments reported here, using time-of-flight measurements as the waves traveled between streamwise-separated sensors. Eight second records were digitized at 1000 Hz on several sensors for given forcing conditions. Cross-correlations of these periodic records were computed in order to determine the average delay time between the arrival of the signal at the first sensor and its arrival at the second.

The phase speed results are given in Fig. 8. These experimental values are slightly higher than those given by the flat-plate, parallel-flow linear theory (see Fig. 9), but the agreement is acceptable, considering that the linear theory has not been corrected for the leading-edge pressure gradient, and does not contain nonparallel flow corrections, and considering that the experimental Reynolds number is only accurate to a few percent. The data for the lower forcing amplitudes are similar, except that they generally have more scatter due to the less coherent waves that are generated. The data at lower Reynolds number that were obtained farther upstream yielded higher phase speeds, with smaller cross-correlations and more scatter. Such a decrease of phase speed with increasing Reynolds number is predicted by the linear theory, as is a slight increase of phase speed with increasing frequency.

The very slight increase in phase speed with increasing wave angle that is evident in Fig. 8 is consistent with Squire's theorem [for the temporal case; see Ref. 14, Eq. (25)]. For 2-D linear parallel-flow instability waves, an equation $F(\alpha,R,c)=0$ relates the complex eigenvalue c to the Reynolds number R and the wave number α. Squire's theorem states that this relation for c, and thus the phase speed, can also be used for oblique waves of spanwise wave

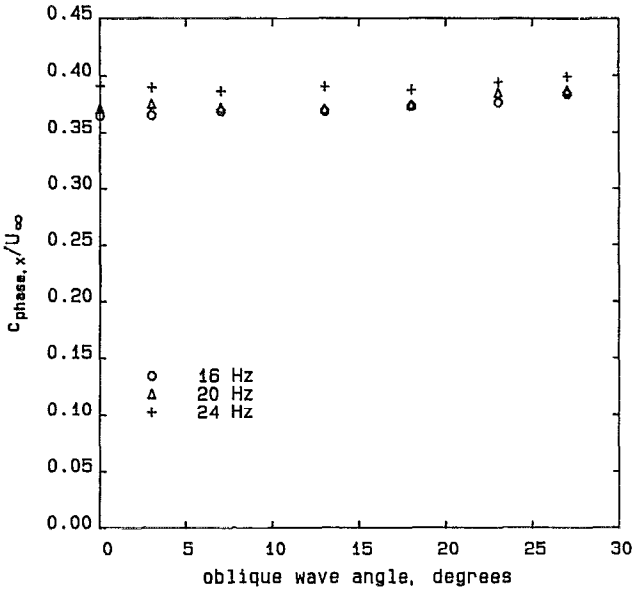

FIG. 8. Streamwise phase speeds at $Re_{\delta*}=1400$. Here $U_\infty=1.12$ m/s, streamwise spacing of 34.93 mm, 192 W, sensors S5 and S7, $Re_{\delta*}(S5)=1350$, $Re_{\delta*}(S7)=1400$.

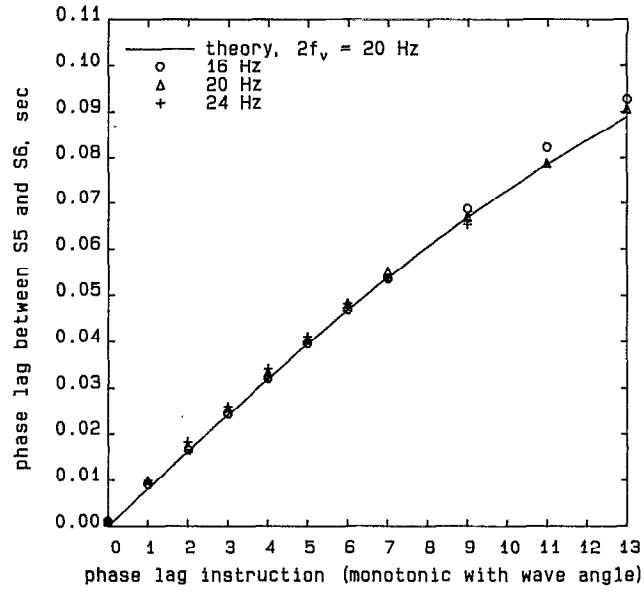

FIG. 10. Average phase shifts against angle for oblique waves. Sensors S5 and S6, $U_\infty=1.07$ m/s, 192 W, $Re_{\delta*}=1300$, phase lag instruction 13 is 31° waves. Theory uses $c_{phase,x}=0.38U_\infty$.

number β, if one uses the transformation $\bar{\alpha}=\sqrt{\alpha^2+\beta^2}$ and $\bar{R}\bar{\alpha}=R\alpha$. It is important to note that in both cases $c=\omega/\alpha$, so that in both cases the real part of c is the streamwise phase speed. Thus, the phase speed of a given oblique wave is the same as the phase speed of a 2-D wave with a higher streamwise wave number and a lower Reynolds number. Since the theoretical phase speeds for the temporal case increase with decreasing Reynolds number and increasing streamwise wave number (see, for example, Wazzan *et al.*[39]), the theory agrees with the experimental result that the streamwise phase speed increases with angle.

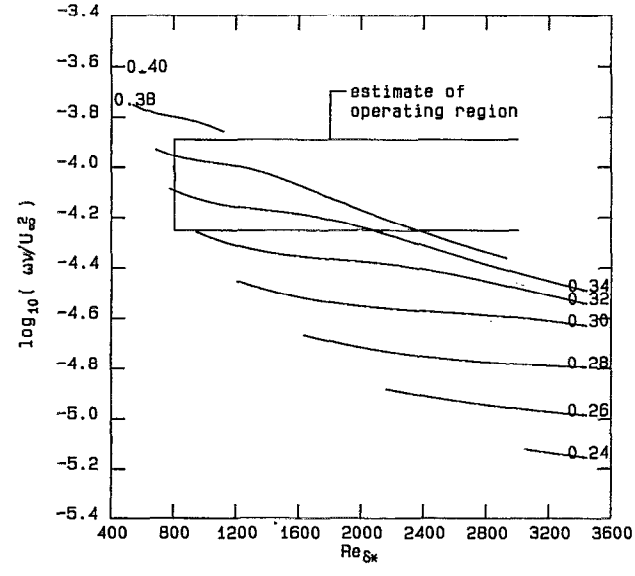

FIG. 9. Streamwise phase speeds from linear theory for parallel flow. Contours of $c_{phase,x}/U_\infty$ at 0.02 intervals. The 2-D linear theory results are from Mack.

Computations for the spatial-case linear theory supplied by Mack also show an increase of the streamwise phase speed, which for oblique waves of angle 30° is about 5% above the 2-D value. The experimental data show that the phase speed increases about 0.02 as the obliquity increases between 0° and 30°, an increase that is also about 5% above the 2-D value. These results are substantially in agreement with those inferred by Seifert from spectral processing of wave-packet data (Ref. 40, p. 24).

This change of phase speed with the angle for oblique waves was previously measured by Kachanov (Ref. 17, Figs. 4 and 5), using a vibrating-ribbon generator at two oblique angles. His results show a decrease in phase speed with increasing wave angle, the opposite trend to that reported here; but his measurements refer to the x component of the phase speed, $\omega\alpha/(\alpha^2+\beta^2)$. When his data are replotted in the same form as given here, their trend with angle is the same as that observed here.[41] He also reports an increase of phase speed with increasing frequency, in agreement with the trend reported here.

C. Measured angles

The angles of the oblique waves were measured using data from sensors spaced in the spanwise direction at the same streamwise location. The phase lag of wave arrival at the different spanwise locations determines the angle. The method of computing the phase lag is the same as that used for the phase-speed analysis above. The results for the phase shift are given in Fig. 10.

IV. NONLINEAR OBLIQUE WAVES

The instability waves grow along the plate until they become nonlinear, a term here defined in terms of the wall-shear spectra. Both subharmonics and second and third

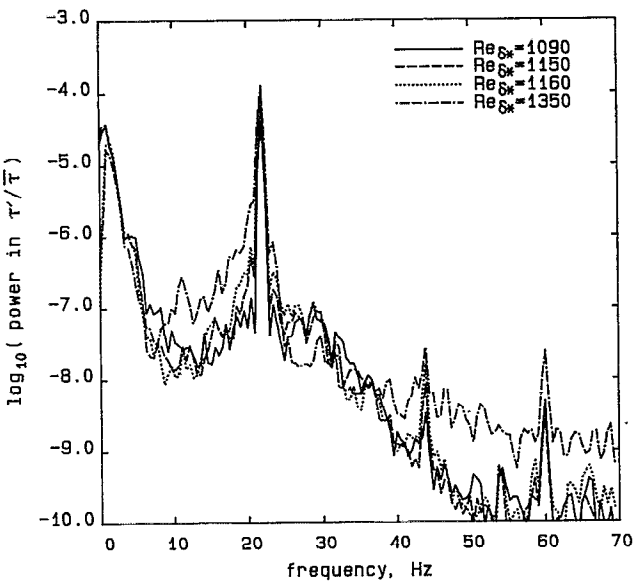

FIG. 11. Early development of nonlinearity in wall-shear spectra. Centerline sensors, $U_\infty = 1.12$ m/s, 192 W, 22 Hz 2-D waves.

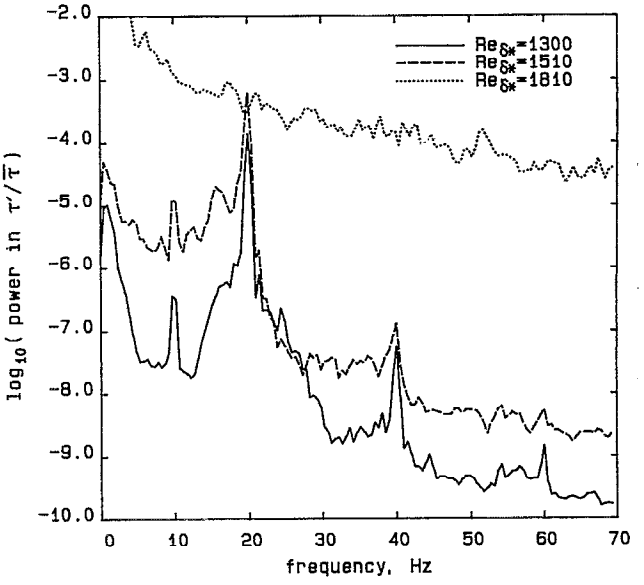

FIG. 12. Development of subharmonic nonlinearity in wall-shear spectra. Centerline sensors, $U_\infty = 1.05$ m/s, 74 W, 20 Hz 2-D waves.

harmonics were observed at various locations, as well as $\frac{3}{2}$ harmonics. Results for these different harmonics are presented in the following sections. It should be emphasized that simultaneous data were always recorded on four sensors. The farthest upstream of the four sensors always yielded small-amplitude wall-shear traces that showed no sign of nonlinear behavior. In Fig. 6, for example, any subharmonic content in the 20 Hz wave is at least 2.5 orders of magnitude smaller in power. In short, all nonlinear behavior described here occurred after the decay of any nonlinearities that might be present in the flow near the perturbing upstream heater. The nonlinear behavior that occurs downstream is not caused by nonlinearity in the perturbation process, although small perturbations that remain from disturbance nonlinearity may serve as *seeds* that influence the later course of nonlinear amplification.

Figure 11 shows the early development of nonlinearity. At the farthest upstream sensor, the second harmonic is possibly present just above the noise, at 44 Hz. Both the primary- and second-harmonic responses grow monotonically downstream. At the farthest downstream sensor, a subharmonic is just beginning to appear above the background, as part of a general increase in low-frequency activity.

Figure 12 shows the later development of nonlinearity, in a case where subharmonics appear. At $\mathrm{Re}_{\delta^*} = 1300$, the subharmonic has appeared above the background, being slightly larger than the small subharmonic in the previous figure. Farther downstream, at $\mathrm{Re}_{\delta^*} = 1510$, the subharmonic is more energetic, with a general filling in of the low-frequency part of the spectrum. At the farthest downstream sensor, the flow has become intermittent, with large local fluctuations, and the spectrum is broadband. The nonlinearities at $\mathrm{Re}_{\delta^*} = 1300$ are comparable to those at 1350 in the previous figure, even though the heater power is lower. This is probably due primarily to the somewhat larger primary-wave amplitude encountered at the more-amplified frequency of 20 Hz.

Figure 13 shows the spectrum of a strongly nonlinear signal. The peak amplitude of the 20 Hz fundamental is about 2.5%. Not only is there a strong subharmonic and second harmonic, but nonlinearly generated $\frac{3}{2}$ and $\frac{5}{2}$ harmonics appear. The response at 60 Hz is at least partly due to line noise. The nonlinearity is stronger than in the previous figures, because the primary wave is much larger, due to the larger heater power and the more-amplified generation frequency.

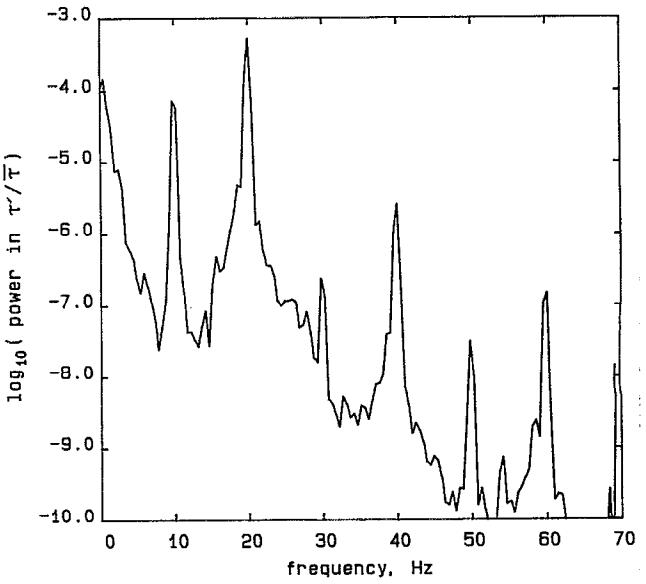

FIG. 13. Wall-shear spectra showing large nonlinearities. We see 20 Hz waves, sensor S4, $U_\infty = 1.07$ m/s, $\mathrm{Re}_{\delta^*} = 1300$, 192 W, 2-D waves.

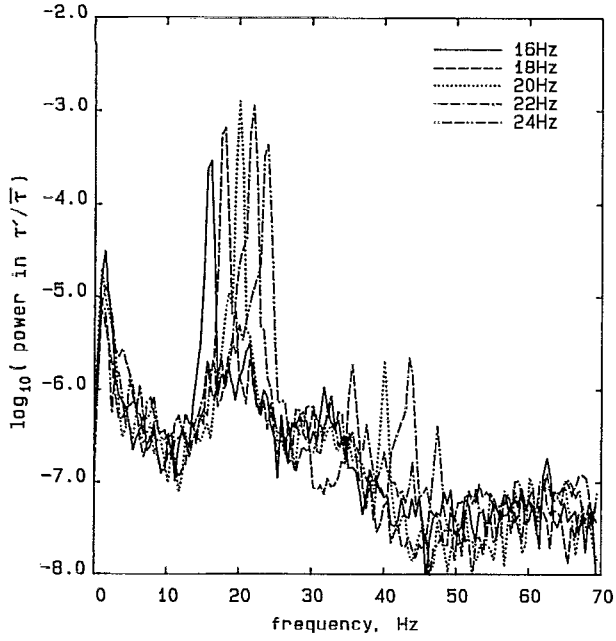

FIG. 14. Wall-shear spectra showing second harmonics. Sensor S7, $Re_{\delta*}=1400$, $U_\infty=1.12$ m/s, 192 W, 2-D waves.

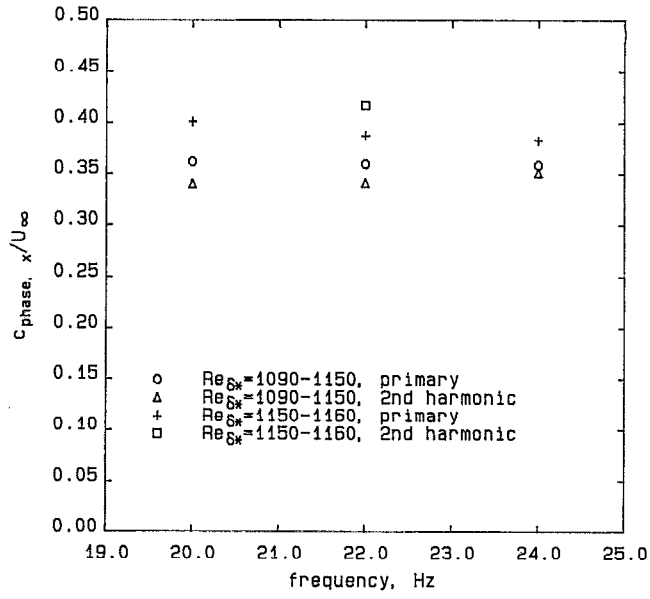

FIG. 16. Phase speed of primary and of second harmonic. We see 2-D waves, $U_\infty=1.12$ m/s, centerline sensors, 192 W.

A. Higher harmonics

Second harmonics are always seen on all sensors located in the nonlinear region, and are, in fact, the clearest sign that the waves have entered the nonlinear region. A typical set of spectra showing second harmonics only is shown in Fig. 14. The figure shows spectra for five separate experiments. Second harmonics are visible for all five frequencies.

At smaller amplitudes of the primary wave, the harmonics are also smaller. Figure 15 shows the amplitude of the second-harmonic wave plotted against the square of the amplitude of the primary wave for 20 Hz waves of various oblique angles with differing initial perturbation amplitudes. It can be seen that the second harmonic increases quadratically with the primary response, as might be expected if it is caused by a simple nonlinear interaction. If the shear consists of a single harmonic,

$$\tau=\epsilon \sin \omega t,$$

then a quadratic nonlinearity that goes like $c_0\tau^2$ will produce a signal,

$$\tau=\epsilon \sin \omega t+\frac{c_0\epsilon^2}{2}(1-\cos 2\omega t).$$

Plotting the square of the amplitude of the fundamental against the amplitude of the second harmonic should then give a linear curve. It is also evident from the figure that there is no marked variation of the coefficient c_0 with the oblique wave angle, at least for small angles. Other data show that this second harmonic persists with increasing angle, remaining at a nearly constant ratio to the primary, even for angles larger than those plotted in Fig. 15.

Figure 16 shows the phase speeds of the second harmonics along with those of the primary 2-D waves. The phase speeds of the second harmonics are obtained by digitally filtering the data using a 4 Hz bandwidth, and then processing as for the case of phase speeds in the linear region. The data are plotted for three values of the primary frequency for two different sensor combinations. It can be seen that the signal called the second harmonic has a phase speed nearly equal to that of the primary. If this signal were linearly independent of the primary, it would be expected to have a phase speed roughly 20% higher than that of the primary, since the frequency is twice that of the

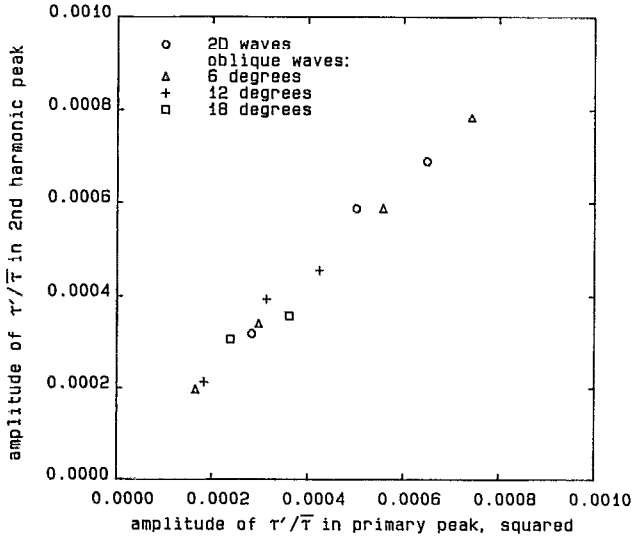

FIG. 15. Amplitude of second harmonic against amplitude of primary. We see 20 Hz, sensor S6, $Re_{\delta*}=1300$, varied heater power, $U_\infty=1.07$ m/s.

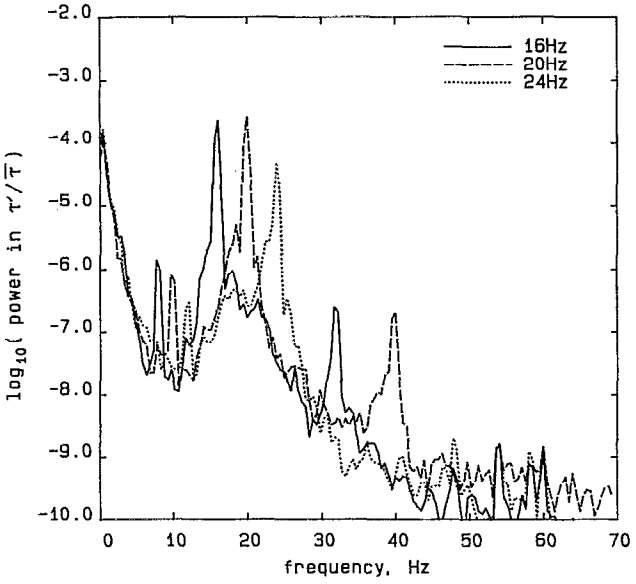

FIG. 17. Wall-shear spectra showing subharmonics. Sensor S4, $Re_{\delta^*}=1300$, $U_\infty=1.07$ m/s, 6° oblique waves, 192 W.

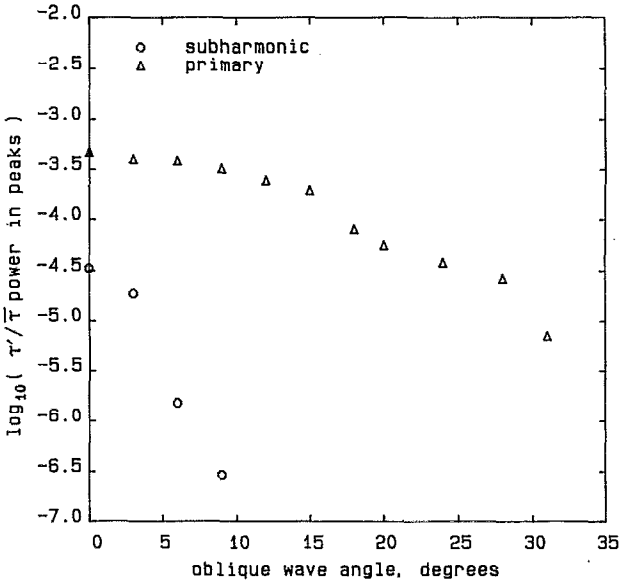

FIG. 18. Decrease in subharmonic amplitude with angle. We see 20 Hz, 192 W forcing, sensor S4, $Re_{\delta^*}=1300$, $U_\infty=1.07$ m/s.

primary (see Fig. 9). Instead, the phase speed matches that of the primary, due to nonlinear phase locking of the two frequencies.

It was hoped that study of the second harmonic would provide a clear indication of the primary amplitude at which the wave becomes nonlinear (through some sudden change in the behavior of the second harmonic at a threshold value of the primary). However, the evidence is that the amplitude of the second harmonic increases slowly with the amplitude of the primary, the amplitude at which it first becomes visible being dependent only on the noise level in the spectra. Thus, the development of nonlinearity is a continuous process, at least insofar as the second harmonic is concerned. This smooth development of the second harmonic can also be seen in the experimental results of Kachanov *et al.* [Ref. 42, Fig. 4(d)], and in Kleiser's numerical results (Ref. 43, Fig. 12).

B. Subharmonics

Subharmonics are often seen on the sensors in the nonlinear region, starting downstream of the region where the second harmonic is first seen. The subharmonic frequency suggests the local existence of the staggered Λ-vortex pattern (Fig. 1), and appears to arise spontaneously from the background noise in the flow. Figure 17 shows a typical set of spectra, for three different forcing frequencies. The subharmonics appear with or downstream of the second harmonics. Subharmonics are not seen uniformly at all spanwise locations, but seem to vary in amplitude across the span in a unpredictable fashion, the location where they are seen differing from day to day, but remaining the same over the course of a day. This behavior is probably an indication of a mixed transition pattern, with some of the lambda vortices being in line and some staggered, and with the pattern varying across the span.[1] Such a mixed pattern is to be expected when the nonlinear instability develops from random background noise. It was observed by Spalart and Yang [Ref. 44, Fig. 2(h)], who used random background noise to generate the three-dimensionality. Kachanov [Ref. 7, Fig. 14(b)], who also allowed the secondary instability to develop from natural disturbances, reports a variation of subharmonic amplitude with spanwise position large enough that the subharmonic vanishes at the spanwise node of the staggered pattern. Thus, one expects irregularities in the spanwise locations of the subharmonics, although these spanwise locations could be fixed if they are locked to small fixed three-dimensional nonuniformities in the free-stream flow or in the heaters.

It should be noted that the DC offset error in the sinusoidal heater voltage signals provides a weak subharmonic perturbation of about 2% of the primary perturbation. Also, the subharmonic frequency of 10 Hz falls in an amplified region of the parallel flow linear instability diagram. Thus, the strength of the subharmonic may have involved weak seeding and some linear amplification. Last, the primary wave amplitude is large because of the forcing (about $10^{-3.3/2}$ or 2.2%), and so the nonlinear wave behavior is not surprising, despite the low Reynolds number of the flow at the sensor.

Figure 18 shows typical results for the amplitude of the primary- and subharmonic response, for various angles of obliquity. At all measurement locations, the amplitude of the oblique waves at the primary frequency decreased with increasing obliquity. The amplitude versus angle curve has zero slope at zero degrees, as might be expected from Squire's theorem.[14] The oblique waves at larger angles remain clearly smaller than the 2-D waves as the wave amplitude increases, at least up to wave amplitudes of a few percent of the mean shear.

The most interesting observation is that when subhar-

monics are seen, they are strongest for 2-D forcing, and decrease rapidly in amplitude for forcing of increasing oblique angle, so that for an oblique wave of perhaps 10° the subharmonic amplitude has decreased by an order of magnitude from the 2-D value (Fig. 18). Never do the subharmonics increase with increasing angle, and therefore it is unlikely that the pattern is simply moving spanwise. This rapid decrease with increasing angle was observed in all cases where subharmonics were observed.

In current nonlinear models, the instability of a strong two-dimensional primary wave is studied. The parametric resonances or secondary instabilities all rely on the spanwise uniformity of the primary wave. Here we have seen that when the obliquity of a strong single-frequency fundamental wave is varied from zero to a small oblique angle, the secondary instability changes. It is not surprising that the subharmonic instability disappears as the primary wave becomes oblique, for one would expect changes in the secondary instability as the spanwise symmetry of the 2-D wave disappears. The rapid but smooth decrease of the subharmonic with small but finite increases in primary wave obliquity is a strong indication that the subharmonic stability is present only for 2-D and near-2-D primary waves.

V. OBLIQUE WAVE BREAKDOWN: THE INTERMITTENT REGION

Eventually the waves break down into turbulent spots, leading to intermittency of the classical kind (Narasimha[45]). Figure 19 shows two flow-visualization images from this region, obtained using dye bled into the boundary layer through small holes. Flow is from left to right, and the dye is visible as the dark, thin, horizontal bands. The dark vertical bands are joints between the sections of the plate, and the dark circle in the center of each image marks the location of a downstream sensor. The flow is laminar in regions where the dye remains near the wall, and turbulent in regions where the dye has been washed away. The interface is ragged and unsteady. The interface moves upstream markedly when significant forcing is turned on, corresponding to an upstream movement of transition.

The dye visualized in these images is located too close to the wall to show the structure of the subharmonic instability. Other workers have been able to visualize this structure, using smoke wires in air.[8,46] Preliminary experiments with hydrogen-bubble wires in our water flow encountered difficulties with bubble accumulation on the lower, working surface of the plate. Reorientation of the place was not feasible because of problems with waves on the free surface and with tunnel access and cable routing. An attempt was made to obtain schlieren visualizations similar to those in Ref. 21, but the slow boundary-layer growth scales made this impractical.

If a sensor is placed in the fluctuating region shown in Fig. 19, the fraction of time when the flow is turbulent can be computed (see Ref. 26 for details). This fraction, known as the intermittency, increases with downstream distance until the flow is fully turbulent. Here, the intermittency was measured at a fixed sensor, and the intermittency was observed to increase with increased amplitude of forcing. Thus, the intermittency measurements confirmed the flow visualization and showed that the transition point moved upstream with increased forcing.

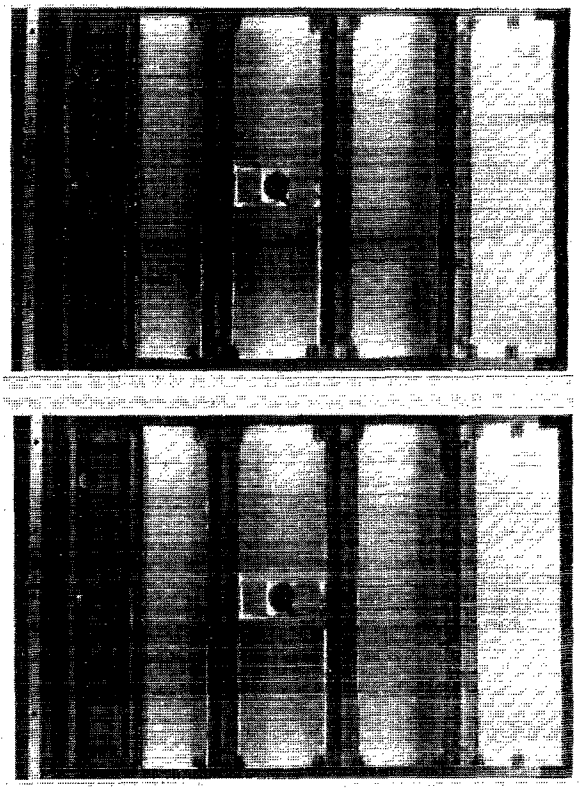

FIG. 19. Visualizations of transition, with and without forcing. Upper photo: unforced. Lower photo: forced 16 Hz, 192 W, 12° oblique waves. Both photos: $U_\infty = 1.07$ m/s, flow from left to right.

Extensive experiments were done with oblique wave forcing in order to get the intermittency to converge to an average that is precise enough to resolve the effects of the oblique-wave angle. The intermittency was computed for five successive records of about 300 instability-wave cycles each. The RMS variation of these five values of the intermittency about the mean was about 0.1, indicating that the record lengths were sufficient to obtain a value for the intermittency that has converged to within a statistical variation of less than 0.1. The mean intermittency is plotted in Fig. 20, which shows that as the angle of oblique wave forcing is increased, the transition point moves upstream less and less. The reduced intermittency for the 2-D waves, as compared to the 5° or 10° waves, is almost certainly due to the 13% smaller amplitude of the 2-D wave generation that was noted earlier. Thus two-dimensional forcing has the largest effect on the movement of the transition point. It is important to remember that this forcing is located at a fixed streamwise location, near the critical Reynolds number.

This result is not surprising, in view of the generally smaller oblique wave amplitudes measured at the end of the linear region. The nonlinear effects that favor the

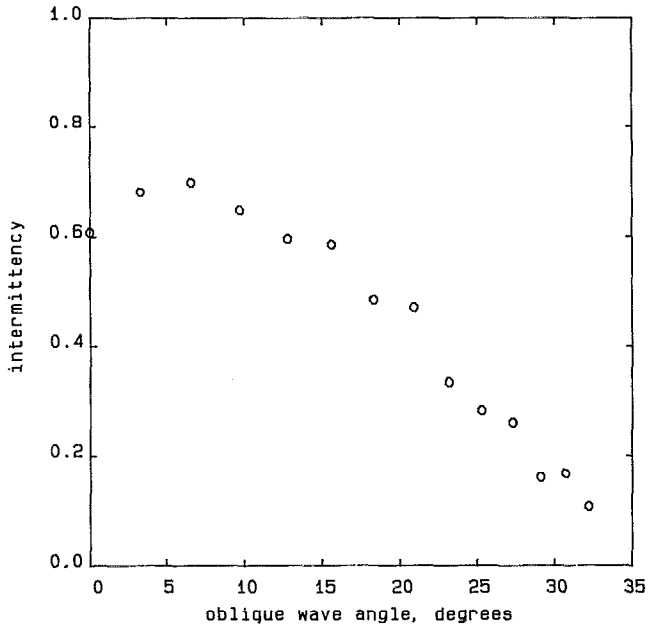

FIG. 20. Effect of wave obliquity on transition. We see 20 Hz, 163 W forcing, $U_\infty = 1.12$ m/s, centerline sensor, 80 s record, $Re_x = 1.1 \times 10^6$.

growth of oblique waves, discussed in the Introduction, are evidently not sufficient to overcome their smaller linear growth rates and possibly weaker receptivity to the heating. This experiment provides the first observations of the development of oblique waves all the way into the intermittent region.

VI. SUMMARY OF RESULTS

Development of three-dimensionality in the laminar–turbulent transition of boundary layers has recently been a subject of a great deal of research, much of which involves study of the nonlinear breakdown of large-amplitude 2-D primary waves. Two different mechanisms have been recognized as part of this process. One involves spanwise disturbances that are arranged in a staggered pattern. This staggered pattern can be explained using resonance between a 2-D primary wave and a pair of oblique waves of equal and opposite angle. However, such flows are all spanwise periodic and symmetric.

In the present paper, we address a different topic; namely, the breakdown of large-amplitude single *oblique* primary waves. This flow is no longer spanwise symmetric, although it is still spanwise periodic. A new apparatus for exploring the growth of single oblique laminar instability waves has been developed from the apparatus of Robey.[20] This new apparatus has improved the accuracy of wave generation by an order of magnitude both in phase and in amplitude. Downstream development of single oblique instability waves was studied for various wave angles, amplitudes, and frequencies, using fixed wall-shear sensors.

The emphasis in the research was on the nonlinear development of single oblique waves. The amplitude of second harmonics in the wall shear response was observed to scale with the square of the primary amplitude. Subharmonics were also observed, in what was apparently a mixed transition pattern, since they were not uniformly present at all spanwise locations. When subharmonics were observed, their amplitude was largest for 2-D forcing and decreased rapidly with increasing oblique angle, decreasing by an order of magnitude as the oblique angle was increased from 0° to 10° (Fig. 18). This result suggests that the nonlinear secondary instability of even slightly oblique waves is different from that of 2-D waves. It is conjectured that this difference is associated with the loss of spanwise symmetry that is inherent in the wave obliquity. Since 2-D waves and small-angle oblique waves will both occur in a real flow having some natural large-scale three-dimensionality, and will have a very similar growth rate, the possibility of a difference in their breakdown mechanisms deserves further study.

It might be expected that oblique waves become nonlinearly unstable at lower amplitudes than 2-D waves, because they contain all three components of vorticity, and are thus subject to vortex tilting and stretching effects, and because the maximum of vorticity moves away from the wall. Measurements supporting this view were presented by Robey.[11] However, measurements of intermittency at a fixed downstream location show that 2-D forcing, carried out near the beginning of linear instability, causes the largest upstream displacement of the transition point; this upstream displacement then decreases with increasing oblique angle. Thus, nonlinear effects are not sufficient to overcome the larger amplitude that the 2-D waves had at the end of the linear region.

A final conclusion follows from a comparison of the subharmonic and intermittency results (Figs. 18 and 20). As the oblique wave angle is increased, there is an indication of a rapid change in nonlinear breakdown mechanism, but there is no corresponding rapid change in the movement of the transition point.

ACKNOWLEDGMENTS

This work was carried out at the Graduate Aeronautical Laboratories, California Institute of Technology. The first author gratefully acknowledges the advice and support of his thesis advisors, H. W. Liepmann and D. Coles, and the GALCIT community. Dr. James Kendall of the Jet Propulsion Laboratory provided useful comments on several drafts of the manuscript. The work was funded by the Office of Naval Research, under Contract Nos. N00014-85-K-0205 and N00014-87-K-0100.

[1] T. Herbert, "Secondary instability of boundary layers," Annu. Rev. Fluid Mech. **20**, 487 (1988).
[2] L. Kleiser and T. Zang, "Numerical simulation of transition in wall-bounded shear flows," Annu. Rev. Fluid Mech. **23**, 495 (1991).
[3] F. P. Bertolotti, "Linear and nonlinear stability of boundary layers with streamwise varying properties," Ph.D. thesis, Ohio State University, 1990.
[4] P. S. Klebanoff, K. D. Tidstrom, and L. M. Sargent, "The three-dimensional nature of boundary-layer instability," J. Fluid Mech. **12**, 1 (1962).
[5] J. M. Cimbala, H. M. Nagib, and A. Roshko, "Large structure in the far wakes of two-dimensional bluff bodies," J. Fluid Mech. **190**, 265 (1988).

[6]A. Craik, "Nonlinear resonant instability in boundary layers," J. Fluid Mech. **50**, 393 (1971).
[7]Yu. S. Kachanov and V. Ya. Levchenko, "The resonant interaction of disturbances at the laminar–turbulent transition in a boundary layer," J. Fluid Mech. **138**, 209 (1984).
[8]T. C. Corke and R. A. Mangano, "Growth of three-dimensional modes in Blasius boundary layers," J. Fluid Mech. **209**, 93 (1989).
[9]Yu. I. Bublikov and V. M. Fomichev, "Development of oblique waves in a two-dimensional subsonic boundary layer," J. Appl. Mech. Tech. Phys. **33**, 350 (1992) (a translated version of Prikl. Mekh. Tekh. Fiz.).
[10]C. H. K. Williamson, "Defining a universal and continuous Strouhal–Reynolds number relationship for the laminar vortex shedding of a circular cylinder," Phys. Fluids **31**, 2742 (1988).
[11]H. F. Robey, "On the nature of oblique instability waves in boundary layer transition, in *Turbulence Management and Relaminarization*, edited by H. Liepmann and R. Narasimha Proceedings of the IUTAM Symposium, Bangalore, India (Springer-Verlag, New York, 1987), pp. 187–198.
[12]M. Gaster, "A theoretical model of a wave packet in the boundary layer on a flat plate," Proc. R. Soc. London Ser. A **347**, 271 (1975).
[13]I. Wygnanski, J. H. Haritonidis, and R. E. Kaplan, "On a Tollmien–Schlichting wave packet produced by a turbulent spot," J. Fluid Mech. **92**, 505 (1979).
[14]H. B. Squire, "On the stability for three-dimensional disturbances of viscous fluid flow between parallel walls," Proc. R. Soc. London Ser. A **142**, 621 (1933).
[15]A. Craik, "Boundary-layer transition: Theory and experiment, in *Laminar–Turbulent Transition*, Proceedings of the 1st IUTAM Symposium, edited by R. Eppler and H. Fasel (Springer-Verlag, New York, 1979), pp. 218–222.
[16]F. R. Hama, U. Rist, U. Konzelmann, E. Laurien, and F. Meyer, "Vorticity field structure associated with the 3-D Tollmien–Schlichting waves," Sādhanā (A journal of the Indian Academy of Sciences) **10**, 321 (1987).
[17]Y. Kachanov, "Development of spatial wave packets in boundary layer," in *Laminar–Turbulent Transition*, Proceedings of the 2nd IUTAM Symposium, Novosibirsk, edited by V. V. Kozlov (Springer-Verlag, New York, 1984), pp. 115–123.
[18]J. M. Kendall, "Supersonic boundary layer stability experiments," in *Boundary Layer Transition Study Group Meeting, Volume II: Session on Boundary Layer Stability*, edited by W. D. McCauley. Aerospace Corporation, Air Force Report No. BSD-TR-67-213, 1967, Vol II.
[19]L. M. Mack, "Instability wave patterns from harmonic point and line sources in laminar boundary layers," in Ref. 17, pp. 125–132.
[20]H. F. Robey, "On the use of a phased heater array for the controlled excitation of arbitrary three-dimensional perturbations in a laminar boundary layer," Exp. Fluids **5**, 33 (1987).
[21]K. Nygaard and A. Glezer, "Evolution of streamwise vortices and generation of small-scale motion in a plane mixing layer," J. Fluid Mech. **231**, 257 (1991).
[22]H. U. Meier and M.-D. Zhou, "The development of acoustic generators and their application as a boundary layer transition control device," Exp. Fluids **11**, 93 (1991).
[23]L. Kral, "Numerical investigation of transition control of a flat plate boundary layer, Ph.D. thesis, The University of Arizona, Tucson, Arizona, 1988. Also see L. Kral and H. Fasel, "Numerical simulation of the control of the three-dimensional transition process in boundary layers," Proceedings of the 3rd IUTAM Symposium on Laminar–Turbulent Transition, Toulouse, France, 1989, in *Laminar–Turbulent Transition* (Springer-Verlag, New York, 1990), pp. 687–692.
[24]S. P. Schneider, "Experimental introduction of controlled complex 3D perturbation patterns in a boundary layer: Some effects on instability and transition," AIAA Paper No. 92-0738, 1992.
[25]T. M. Ward, "The Hydrodynamics Laboratory at the California Institute of Technology," Trans. ASME J. Fluids Eng. **98**, 740 (1976).
[26]S. P. Schneider, "Effects of controlled three-dimensional perturbations on boundary layer transition," Ph.D. thesis, California Institute of Technology, Pasadena, CA, 1989.
[27]J. L. Hess and A. M. O. Smith, "Calculation of potential flow about arbitrary bodies," Prog. Aeronaut. Sci. **8**, 1 (1967).
[28]F. M. White, *Viscous Fluid Flow*, 2nd ed. (McGraw-Hill, New York, 1992).
[29]G. L. Brown, "Theory and application of heated films for skin friction measurement," in *Proceedings of the 1967 Heat Transfer and Fluid Mechanics Institute* (Stanford University Press, Stanford, CA, 1967), pp. 362–381.
[30]L. M. Mack, "Computations of spatial case linear instability theory for low Reynolds number boundary layers" (Private communication of results for various frequencies, spanwise wave numbers, and Reynolds numbers, 1986–1988).
[31]H. F. Robey, "On the nature of oblique instability waves in boundary layer transition," Ph.D. thesis, California Institute of Technology, Pasadena, CA, 1986.
[32]H. Fasel and U. Konzelmann, "Non-parallel stability of a flat-plate boundary layer using the complete Navier–Stokes equations," J. Fluid Mech. **221**, 311 (1990).
[33]M. Gaster, "Series representation of the eigenvalues of the Orr–Sommerfeld equation," in *Proceedings of the AGARD Symposium on Laminar–Turbulent Transition, Copenhagen* (AGARD/NATO, Brussels, 1977), AGARD CP-224, pp. 2-1–2-12.
[34]W. C. Reynolds, "Orrsom: A Fortran-IV program for solution of the Orr–Sommerfeld equation," Technical Report No. FM-4, Thermosciences Division, Department of Mechanical Engineering, Stanford University, 1969.
[35]L. M. Mack, "Boundary layer linear stability theory," in *Special Course on Stability and Transition of Laminar Flow*, Advisory Group for Aerospace Research and Development, AGARD Report No. 709, 1984.
[36]G. B. Schubauer and H. K. Skramstad, "Laminar boundary-layer oscillations and stability of laminar flow," J. Aeronaut. Sci. **14**, 69 (1947).
[37]F. P. Bertolotti, Th. Herbert, and P. R. Spalart, "Linear and nonlinear stability of the Blasius boundary layer," J. Fluid Mech. **242**, 441 (1992).
[38]G. B. Whitham, *Linear and Nonlinear Waves* (Wiley–Interscience, New York, 1974).
[39]A. R. Wazzan, T. T. Okamura, and A. M. O. Smith, "Spatial and temporal stability charts for the Falkner–Skan boundary-layer profiles," Report No. DAC-67086, Douglas Aircraft Company, Long Beach, CA, 1968.
[40]A. Seifert, "On the interaction of low amplitude disturbances emanating from discrete points in a Blasius boundary layer," Ph.D. thesis, Tel-Aviv University, 1990.
[41]Y. S. Kachanov (private communication, 1 December 1989). See also "3-D Instability of flat-plate boundary layer. Theory and experiment," by Y. S. Kachanov and A. Michalke (submitted to Eur. J. Mech. Ser. B Fluids).
[42]Y. Kachanov, V. Kozlov, V. Levchenko, and M. Ramazanov, "On the nature of *K*-breakdown of a laminar boundary layer. New experimental data," in Ref. 17, pp. 61–73.
[43]L. Kleiser, "Three-dimensional processes in laminar–turbulent transition," in *Nonlinear Dynamics of Transcritical Flows*, Proceedings of a DFVLR International Colloquium, Bonn, Germany, 1984, edited by H. L. Jordan, H. Oertel and K. Robert (Springer-Verlag, New York, 1985), pp. 123–154
[44]P. R. Spalart and K. Yang, "Numerical study of ribbon-induced transition in Blasius flow," J. Fluid Mech. **178**, 345 (1987).
[45]R. Narasimha, "The laminar-turbulent transition zone in the turbulent boundary layer," Prog. Aerosp. Sci. **22**, 29 (1985).
[46]V. V. Kozlov, V. Ya. Levchenko, and W. S. Saric, "Formation of three-dimensional structures on the transition to turbulence in boundary layers," Fluid Dyn. **19**, 893 (1985).